BBA - Bioenergetics 1863 (2022) 148557

Contents lists available at ScienceDirect

BBA - Bioenergetics

journal homepage: www.elsevier.com/locate/bbabio

Praseodymium trivalent ion is an effective inhibitor of mitochondrial basic amino acids and carnitine/acylcarnitine carriers

Giovanna Incampo [a,1], Nicola Giangregorio [a,b,1], Nicola Gambacorta [c], Orazio Nicolotti [c], Concetta Pacifico [d], Luigi Palmieri [a,b], Annamaria Tonazzi [a,b,*]

[a] Department of Biosciences, Biotechnologies and Biopharmaceutics, University of Bari, Via Orabona 4, 70125 Bari, Italy
[b] CNR Institute of Biomembranes, Bioenergetics and Molecular Biotechnologies (IBIOM), Via Amendola 122/O, 70126 Bari, Italy
[c] Department of Pharmacy-Pharmaceutical Sciences, University of Bari, Via Orabona 4, 70125 Bari, Italy
[d] Department of Chemistry, University of Bari, Via Orabona 4, 70125 Bari, Italy

ARTICLE INFO

Keywords:
Praseodymium
Slc25 family transporters
Mitochondria
Liposomes
Reconstitution
Transport
Inhibitor

ABSTRACT

We herein report the identification of the lantanide praseodymium trivalent ion Pr^{3+} as inhibitor of mitochondrial transporters for basic amino acids and phylogenetically related carriers belonging to the Slc25 family. The inhibitory effect of Pr^{3+} has been tested using mitochondrial transporters reconstituted into liposomes being effective in the micromolar range, acting as a competitive inhibitor of the human basic amino acids carrier (BAC, Slc25A29), the human carnitine/acylcarnitine carrier (CAC, Slc25A20). Furthermore, we provide computational evidence that the complete inhibition of the transport activity of the recombinant proteins is due to the Pr^{3+} coordination to key acidic residues of the matrix salt bridge network. Besides being used as a first choice stop inhibitor for functional studies in vitro of mitochondrial carriers reconstituted in proteoliposomes, Pr^{3+} might also represent a useful tool for structural studies of the mitochondrial carrier family.

1. Introduction

Transporters belonging to the Slc25 family are the most numerous among solute carriers, comprising 53 genes in the human genome. The so-called “mitochondrial carrier family” (MCF) allows the continuous flux of metabolites between mitochondria and cytosol to cope with subcellular enzymes compartmentalization. All Slc25 members have common sequence features: a tripartite structure, a 3-fold repeated signature motif, and six transmembrane α-helices (two in each of the three repeats). This common signature strictly characterizes MCF despite the large variety of metabolites translocated, ranging from nucleotides to amino acids, organic and inorganic acids and coenzymes. This, together with the relatively small size of the MCF proteins (about 300 amino acids in length), points to a common mechanism of transport which has been unveiled by crystallographic studies of the mitochondrial ADP/ATP carrier [1,2]. Functional and structural studies of the ADP/ATP carrier were greatly fostered by its high natural abundance, in the inner mitochondrial membrane, as well as the by the availability of specific inhibitors. The discovery of the strong competitive inhibitor atractyloside (ATR) was crucial for the identification and characterization of the mitochondrial ADP/ATP carrier [3]. ATR and the chemically related compound carboxyatractyloside (CATR) lock the carrier in cytoplasmic-open state (c-state) in which the substrate-binding site is open to the mitochondrial intermembrane space [1]. Another class of inhibitors, which includes bongkrekic acid (BKA) and isobongkrekic acid, lock the carrier in the matrix-open state (m-state) in which the substrate-binding site is open to the mitochondrial matrix [4]. Most of the available structural information for the Slc25 family come from the structures of the ADP/ATP carrier in complex with either (C) ATR [1] or BKA [4] which are the sole structures of MCF proteins that have been hitherto solved at the atomic level. From a functional point of view, the transport mechanism of these carriers relies on the alternating exposition of the substrate-binding site either towards the intermembrane space or the mitochondrial matrix. This occurs via the transition between the c-state and the m-state of the carriers and the passage through the “occluded state” in which two “gates” block the access of substrate

Abbreviations: Slc25, solute carrier family 25; MCF, mitochondrial carrier family; ANT, adenine nucleotide translocator; PLP, pyridoxal phosphate; IPTG, isopropil-β-D-1-tiogalattopiranoside; NEM, N-ethylmaleimide; DTE, 1,4-dithioerythritol.

* Corresponding author at: CNR Institute of Biomembranes, Bioenergetics and Molecular Biotechnologies (IBIOM), Via Amendola 122/O, 70126 Bari, Italy.
E-mail address: a.tonazzi@ibiom.cnr.it (A. Tonazzi).

[1] These authors contributed equally to this work.

https://doi.org/10.1016/j.bbabio.2022.148557
Received 13 January 2022; Received in revised form 18 March 2022; Accepted 25 March 2022
Available online 1 April 2022

on both membrane side of the transporter. These gates are constituted by two charged networks, facing the translocation cavity. One gate (cytosolic gate) is positioned towards to the intermembrane space/cytosol. It occurs when the second and fifth residue of the conserved signature motif [YF][**DE**]xx[**KR**], present in each even-numbered α-helix, form ionic bonds between the helices leading to the "cytosolic salt-bridge network" creation. This arranges the carrier in the m-state, with the binding site facing the matrix. The other gate (matrix gate) is positioned just below the substrate binding site and towards the mitochondrial matrix. It occurs when the third and sixth residues of the conserved signature motif Px[***DE***]xx**[KR]**, present in each odd-numbered α-helix, form ionic bonds between the α-helices, leading to the formation of the "matrix salt-bridge network", see Fig. 1(A–F). This arranges the carrier in the c-state conformation, with the binding site exposed to the cytosol. The formation and the break of the ionic bonds between the charged residues of the gates is essential for the transport catalysis, for a review see [5,6]. The functional study of the mitochondrial transporters is based on the proteins reconstitution in liposomes [7,8] and the uptake of specific radiolabeled substrates as function of the time. The transport activity is measured using the "inhibitor stop method" [9]. This procedure requires a rapid and strong inhibitor of the transporter. In fact, "stop inhibitors" greatly vary according to the protein; they range from substrate analogues, like butylmalonate or 1,2,3-benzenetricarboxylate for the dicarboxylate carrier (DIC) and the tricarboxylate carrier (CIC), respectively [10] and references therein, to specific ligands like BKA and CATR as in the case of the ADP/ATP carrier (ANC). When specific inhibitors are not available, more generic reagents, such as sulfhydryl reagents (mersalyl, p-chloromercuribenzenesulfonate, mercuric chloride, and N-ethylmaleimide) or the lysine reagent pyridoxal 5-phosphate (PLP) are used. The well-established strategy based on heterologous gene Expression, Purification, Reconstitution and transport Assays "EPRA", led to many MCF members identification and characterization in terms of substrate specificity and kinetic parameters [11]. Nowadays almost one third among all MCF members still await deorphanization due to obstacles encountered in the EPRA process, for example during the "transport assay", where one limitation can be the absence of an efficient stop inhibitor. When the generic stop inhibitors (see above) are ineffective, is of utmost to look for appropriate new efficient inhibitors to allow the detection of the transport activity. Moreover, the research of transporter's inhibitors is also still of great interest for crystallographic studies. In this paper, we focused on praseodymium, a rare lanthanide, currently used in fiber communication, thermometry, germicidal or therapeutically applications [12]. Pr^{3+}, as many Ln^{3+} ions, can have a coordination number among 2–12, but eight-coordinate and nine-coordinate complex are more frequent with oxygen atoms [13]. Furthermore Pr^{3+}, having a little ionic radius (0.99 Å), is classified as "hard Lewis acids" [14] according to HSAB (Hard and Soft Acid Base) concept [15–17]. Our interest about praseodymium was prompted by the early observation, dating back to when ornithine/citrulline mitochondrial carrier was identified, that Pr^{3+} inhibited the ornithine/ornithine exchange [18], nevertheless the rationale behind its interactions with this as well as with other proteins [19] has never been deepened at molecular level. We here demonstrate that praseodymium ion coordinates negative amino acids of the matrix salt bridge gate, at

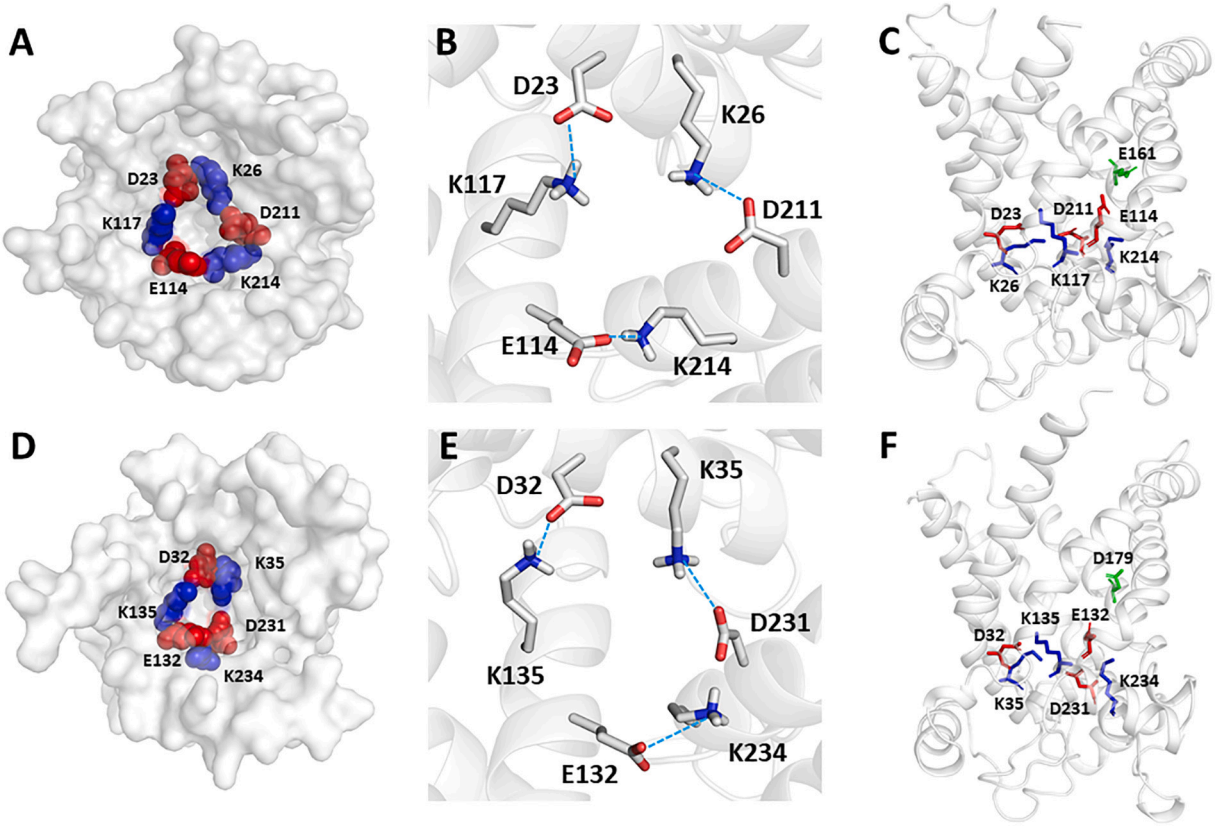

Fig. 1. Residues involved in the matrix salt-bridge network (matrix-gate) of BAC and CAC.
Homology structural models in surface representation from the cytosolic side of BAC (A) and CAC (D). In both, the amino acids belonging to the matrix salt-bridge network, are highlighted as red spheres (negatively charged residues) and blue spheres (positively charged residues). Zoom view of BAC (B) and CAC (E) residues involved in the matrix salt-bridge formation depicted in a stick representation, blue dashed lines highlight the salt bridges. Ribbon diagrams of BAC (C) and CAC (F) in c-state conformation from the lateral side. The residues involved in matrix-salt-bridge network are represented in red stick (negative) and blue stick (positive). Green sticks represent the negatively charged residues of the binding site of BAC (E161) and CAC (D179). The homology structural models have been represented using the molecular visualization program PyMol. (For interpretation of the references to color in this figure legend, the reader is referred to the web version of this article.)

the same time interfering with the binding of the substrate in the active site of some phylogenetically related mitochondrial transporters, and thereby leading to transport inhibition. We demonstrated that this inhibitor does not have any "side effects" on proteoliposomal permeability and can be useful for the transport measurement procedure. More interestingly, it can also represent a useful tool for subsequent crystallization studies.

2. Materials and methods

2.1. Materials

L-[Methyl-^{3}H] carnitine and L-[2,3-^{3}H]ornithine from Scopus Research BV Costerweg. Arginine, L-[2,3,4-^{3}H]-monohydrochloride, from Perkin Elmer Life Sciences Milan, Italy. Sephadex G-75, egg-yolk phospholipids (L-α-phosphatidylcholine from fresh egg yolk), Pipes, Triton X-100, cardiolipin, L-carnitine, L-arginine, and L-ornithine were purchased from Sigma-Aldrich, Milan, Italy. Praseodymium (III) chloride from Alfa Aesar. All other reagents were of analytical grade.

2.2. Overexpression of the human Slc25A29 (BAC), Slc25A20 (CAC) and of Slc25A15 (ORN1) WT proteins

The previously constructed pMW7-WThumanCAC recombinant plasmid was used for producing the human CAC. Bacterial over-expression was obtained transforming *E. coli* C0214 with the recombinant plasmids [20]. The previous constructed pRUN-Slc25A29 recombinant plasmid was used to transform *E. coli* Rosetta-gami B (DE3) (Novagen) strain to produce the corresponding human protein [21]. Recombinant expression plasmid pET-21a(+)-hORC1, encoding a full length hORC1 protein with a His6 tag before the termination codon was used to transform *E. coli* C0214 and obtain bacterial over-expression [22]. In all cases, the cells were collected after 5 h induction by IPTG. Isolation of the inclusion body fraction, solubilization and purification of the proteins were performed as described previously [23].

2.3. Reconstitution of mitochondrial carriers in liposomes

The recombinant proteins, after purification to homogeneity, were reconstituted into liposomes by the detergent removal method, using a column of hydrophobic resin Amberlite XAD-4 [24]. In this procedure, the mixed micelles containing detergent, protein and phospholipids were repeatedly passed through the same Amberlite column (2.8 cm × 0.5 cm). The resin is highly affine for hydrophobic molecule and, at each passage of the reconstitution mixture, gradually removes the detergent molecules allowing the proteoliposomes assembly. The composition of the starting mixture used for reconstitution was: 90 μl 10% Triton X-100; about 0.6 μg purified protein solubilized with 5 μl 5% Sarkosil, 100 μl 10% egg yolk phospholipids in the form of sonicated liposomes; 15 mM of the internal substrate (either arginine, ornithine or carnitine), 20 mM HEPES pH 8 (BAC and ORC1) or 20 mM Pipes pH 7 (CAC); water was added to reach a final volume of 680 μl. After vortexing, the mixture was passed 18 times through the same Amberlite column, equilibrated with 20 mM of the same buffer used in the reconstitution mixture. All the operations were performed at 4 °C, except the passages through Amberlite which were performed at room temperature [23].

2.4. Transport measurements in proteoliposomes

2.4.1. Forward exchange procedure

For transport assay in proteoliposomes, the external substrate was removed from reconstituted proteoliposomes (see Section 2.3) by passing 550 μl of proteoliposomes through a Sephadex G-75 column. The first 600 μl of the turbid eluate from the Sephadex column was collected, transferred to reaction vessels (100 μl each), and readily used for transport measurement by the inhibitor-stop method [25]. For uptake measurements (forward exchange procedure), transport at 25 °C was started by adding 0.1 mM [^{3}H]arginine, [^{3}H]ornithine or [^{3}H]carnitine, to proteoliposomes and at the required time interval, 30 min for dose/response experiments and 5 min for kinetic experiments. The reaction was terminated by the addition of 2 mM NEM (CAC and ORC1) or 15 mM PLP (BAC), or $PrCl_3$ at the indicated concentrations. In controls (blanks), the inhibitor was added together with the labeled substrate at time zero. Finally, the external substrate was removed by chromatography on Sephadex G-75 columns, and the radioactivity in the liposomes was measured. The experimental values were corrected by subtracting blank values.

2.4.2. Backward exchange procedure

For efflux measurements (backward exchange method), the proteoliposomes were loaded with radioactivity before starting the transport assay using the foreword exchange method (see above). This was achieved by incubating the proteoliposomes (600 μl), passed through Sephadex G-75, with 50 μM appropriate labeled substrate with a specific radioactivity of 10 nCi/nmol, for 60 min at 25 °C. Then, the external radioactivity was removed by passing again the proteoliposomes through a second Sephadex G-75 column as described above except that this chromatography was performed at 4 °C to minimize the loss of internal substrate during the chromatography. Transport (efflux) was started by adding external substrate and stopped at the appropriate time interval. The transport assay temperature was 25 °C. Finally, each sample of proteoliposomes (100 μl) was passed through a Sephadex G-75 column to separate the external from the internal radioactivity. Efflux activity was expressed as percentage of intraliposomal radioactivity compared to control at time zero.

2.5. Homology modeling and quality assessment

The three-dimensional (3D) structure of human CAC (Slc25A20) and human BAC (Slc25A29) proteins were obtained using homology modeling method by SWISS MODEL (https://swissmodel.expasy.org/) server using bovine mitochondrial ADP/ATP carrier in complex with carboxyatractyloside as template protein (PDB ID: 1OKC). Sequence identity of CAC (NP_000378.1) and BAC (NP_001034444.1) for ANT is respectively 22.11% and 25.56%. The quality of the models was validated by Qualitative Model Energy Analysis (QMEAN) server (https://swissmodel.expasy.org/qmean/) [26]. The QMEAN score obtained was 0.59 for both proteins. The structures were visualized by PyMOL software. (The PyMOL Molecular Graphics System, Version 2.0 Schrödinger, LLC.) Deepview Alphafold [27] has been also used to get a deeper inspection of the negatively charged residues in the functional part of the proteins.

2.6. Computational studies

Energy minimizations were performed with Prime package [28,29] available on Schrodinger suite. VSGB 2.0 solvation model [30] and OPLS3e force field [31] were employed. The dielectric constant of the solvent was equal to 80 (assuming water as default). A number of 250 iterations of energy minimization was performed along with several updates at the beginning of each iteration, such as on long-range pairs and solvent parameters, in order to avoiding the increase of errors in the minimization; furthermore, 65 steps for each iteration were set: each step involved the application of the conjugate gradient algorithm to obtain a new geometry. The iteration cycle finished when the maximum number of steps was completed. Finally, the RMS gradient threshold for the minimization convergence was set to 0.01 kcal/mol $Å^{-1}$. For the sake of completeness, the X-ray atom type of praseodymium ion was taken from 5AVK [32] crystal structure available from PDB [25].

3. Results

3.1. Kinetics of ORC1, BAC and CAC transporters inhibition by $PrCl_3$

The antiport rate, measured as uptake (forward exchange method), catalyzed by the human isoforms ORC1, BAC and CAC, of 100 μM [^{3}H] ornithine, [^{3}H]arginine or [^{3}H]carnitine into proteoliposomes containing 15 mM ornithine, arginine or carnitine, was determined in the presence of increasing concentration of $PrCl_3$ after 30 min. The dose response curves obtained are shown in Fig. 2. The $PrCl_3$ complete inhibition of the transport was observed for all the carriers at about 2–5 mM. The IC_{50} values calculated for ORC1, BAC and CAC were equal to 522 ± 62 μM, 52.5 ± 8.8 μM and 155 ± 17 μM, respectively (Fig. 2). The differences among the IC_{50} will be deepened in the discussion section. Even though our initial inspiration for the praseodymium utilization come from its effect on ORC1 [33], Pr^{3+} appears a more efficient inhibitor of BAC and CAC. Moreover, the Km value of each carrier for its transported substrate is: 0.16 mM (ORC1), 0.42 mM (BAC) and 0.51 mM (CAC) [21,34,35] so the IC_{50} for ORC1 is higher than the Km for ornithine. Starting from these results, we decided to focus subsequent experiments on the latter two carriers. The dependence of the antiport rate on the external substrate concentration was observed on BAC and CAC, in the absence or presence of the metal. The kinetic experiments were performed measuring the transport activity as initial rate (5 min) and adding 50 μM and 400 μM $PrCl_3$ respectively to the proteoliposomes simultaneously with various concentrations of [^{3}H]arginine or [^{3}H] carnitine [36]. We observed that 400 μM $PrCl_3$, was the optimal concentration to achieve a good inhibition in CAC kinetic experiments, a higher value compared to the IC_{50} (155 μM). We argue because within the 5 min of transport, praseodymium cannot exert its complete inhibition. The data obtained were analyzed in Eadie–Hofstee plots as reported in Fig. 3A–B, and as double reciprocal plots (Lineweaver-Burk) shown in the inserts. Both the representations highlight a competitive inhibition trend for both BAC, Fig. 3A, and CAC, Fig. 3B. The half saturation constant (K_i) for the inhibitor, derived from the Lineweaver-Burk plots, were equal to 28.5 ± 11.7 μM for BAC and to 257.7 ± 71.6 μM for CAC. The observed competitive inhibition may be explained by the binding of Pr^{3+} at, or near, the substrates binding sites.

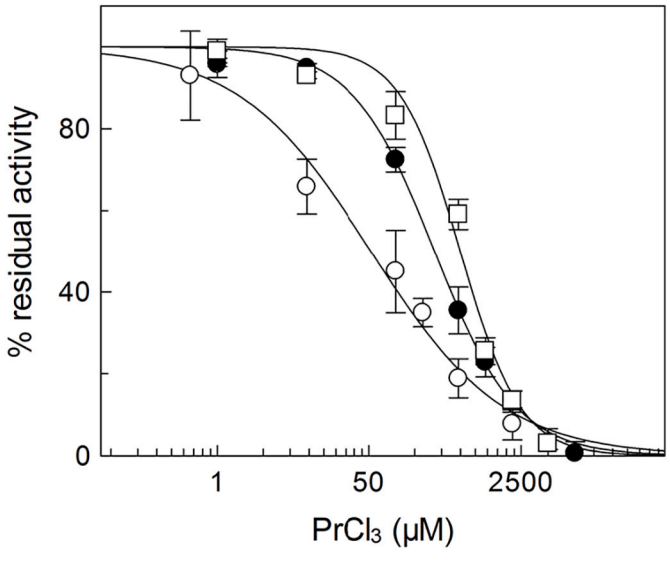

Fig. 2. Dose-response curves for the inhibition of $PrCl_3$ on the reconstituted BAC, CAC and ORC1. The antiport rate was measured adding 0.1 mM [^{3}H] arginine, [^{3}H]carnitine or [^{3}H]ornithine, together with the indicated concentrations of $PrCl_3$ to proteoliposomes reconstituted with BAC (○), CAC (●) or ORC1 (□), respectively. Intraliposomal concentration of each substrate was 15 mM. Percent of residual activity with respect to the control, without $PrCl_3$ treatment, is reported. Transport activity, of control sample, were: BAC 2.5 mmol/g protein/30 min; CAC 0.9 mmol/g protein/30 min and ORC1 0.13 mmol/g protein/30 min. The values are the means ± SD from three independent experiments for BAC and ORC1 and from five independent experiment for CAC.

3.2. Effect of $PrCl_3$ on the [^{3}H] arginine efflux from proteoliposomes

Proteoliposomes, reconstituted with BAC, were loaded with [^{3}H] arginine by transporter-mediated exchange equilibration (see Materials and methods) to measure backward transport activity. This method has here been used to point out the possible Pr^{3+} "side effect" on protein or on the proteoliposomes scaffold that, in the case of some reagents, can lead to specific leakage of labeled substrate. The backward exchange was started adding 5 mM arginine to proteoliposomes pre-loaded with labeled substrate. The control curve fitted a double exponential decay kinetic with the 1st rate constant of 4.52 min^{-1} (Fig. 4, open circles). Addition of 5 mM $PrCl_3$ completely abolished the transport, since no efflux of labeled substrate was observed (Fig. 4, closed circles). This result both confirms praseodymium inhibitory effect, observed in previous experiments, and excludes also the alteration of the proteliposomal scaffold. Addition of the reducing agent DTE (Fig. 4, open squares) did not reverse the inhibition by $PrCl_3$, excluding its coordination binding with pivotal thiol residues important for the transport activity. In the same experiment the addition of 0.5 mM mersalyl induced a prompt [^{3}H]arginine efflux with rate constant of 21.39 min^{-1} (Fig. 4 closed triangle). This phenomenon is not unusual for some MCF members and corresponds to the, so called, "pore-like" activity which is reversed by the addition of DTE (open triangle). The "pore-like" activity on BAC, i.e. the conformational changes of the carrier's structure leading to unspecific labeled arginine leakage, has been here evidenced for the first time, and occurs in several other mitochondrial carriers [33,37–39].

3.3. Insight on the Pr^{3+}/BAC molecular interaction within the matrix gate through energy minimization steps

All the mitochondrial carriers are characterized by a matrix salt-bridge network (matrix gate), composed of three salt bridges involved in the transport catalysis [2]. Since Pr^{3+} forms coordination binding with negatively charged species we performed a computational analysis to verify if the negatively charged residues of the gate could be the target of Pr^{3+}. Four energy minimization simulations were performed on the homology model of BAC as follows: 1) crystal structure of the empty carrier, Fig. 1B depicts key residues within the BAC carrier matrix salt bridge network. After 250 step of energy minimization, the total energy of the system was equal to −10,659.65 kcal/mol; 2) complex of carrier-Pr^{3+}, the latter placed within 3 Å of D23 residue (named BAC-D23-Pr^{3+}) Fig. 5A–D; 3) complex of carrier-Pr^{3+}, the latter placed within 3 Å of E114 residue (named BAC-E114-Pr^{3+}) Fig. 5B–E; and 4) Complex of carrier-Pr^{3+}, the latter placed within 3 Å of D211 residue (named BAC-D211-Pr^{3+}) Fig. 5C–F. The presence of Pr^{3+} ion within 3 Å from the negative charged residues, affects the position of charged couples D23-K117, E114-K214 and D211-K26 and the total energy of the systems. As matter of facts, the energy values returned after 250 steps of energy minimization were equal to −10,858.72 kcal/mol, −11,022.28 kcal/mol and −10,922.59 kcal/mol for BAC-D23-Pr^{3+}, BAC-E114-Pr^{3+} and BAC-D211-Pr^{3+} respectively. For the sake of clarity, all distances between Pr^{3+} and key interacting residues were below 2.5 Å, and thus all the showed coordination bonds were automatically flagged by GLIDE software in agreement with the experimental observations. As shown in Fig. 5, praseodymium ion can coordinate some negatively charged residues other than the ones of matrix salt bridge network Fig. 5D–F. As for BAC-D23-Pr^{3+} complex, Fig. 5D, side chain of D23 can switch its position in order to coordinate Pr^{3+} together with the carbonyl groups of G61 and K60 backbone. Regarding BAC-E114-Pr^{3+}, Fig. 5E, negatively charged side chains of E114 and E161 face each other in order to generate a stable coordination bond with Pr^{3+}. Interestingly, this system

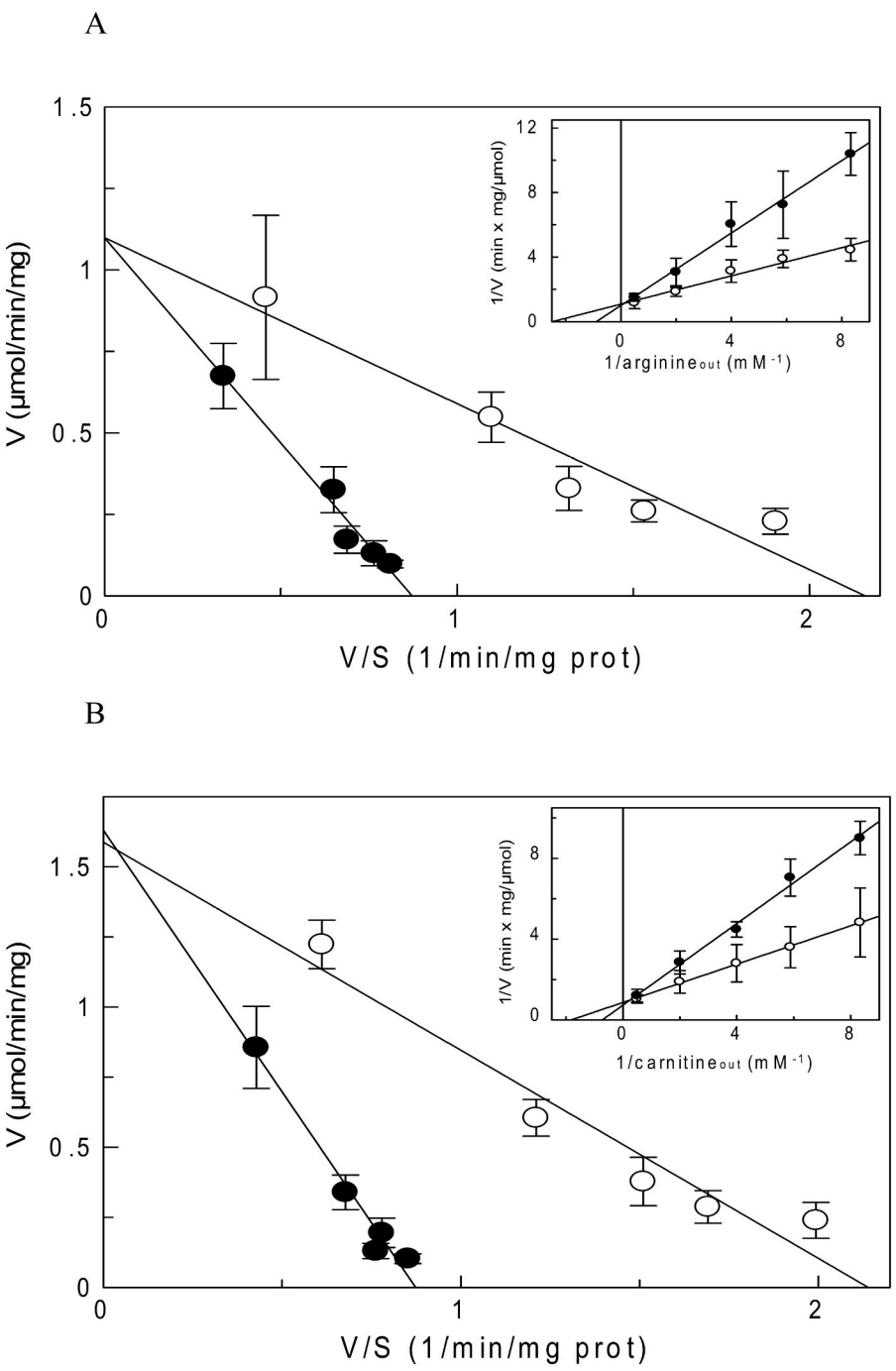

Fig. 3. Kinetic analysis of the inhibition by $PrCl_3$ of the recombinants BAC and CAC. (A) The antiport rate was measured adding [^{3}H]arginine 0.12–0.17–0.25–0.5 –2.0 mM to proteoliposomes containing 15 mM internal arginine, in the absence (○) or in the presence (●) of $PrCl_3$ 50 µM added together with the labeled substrate. (B) The antiport rate was measured adding [^{3}H] carnitine 0.12–0.17–0.25–0.5–2.0 mM to proteoliposomes containing 15 mM internal carnitine, in the absence (○) or in the presence (●) of $PrCl_3$ 400 µM added together with the labeled substrate. Experimental data are plotted according to Eadie Hostee plot. In the insets Lineweaver-Burk as reciprocal transport rate vs reciprocal arginine or carnitine concentrations respectively in A and B. Reported values are means ± S.D. from three independent experiments.

returned the lowest total energy value among all simulations and involved an additional residue, i.e. E161, for better coordinating the Pr^{3+} ion. Eventually, as far as BAC-E211-$Pr^{3+}$is concerned, Fig. 5F, side chain of D211 and the carbonyl group of Q30 backbone can interact with Pr^{3+}, whose presence can displace the positively charged side chain of K26.

3.4. *Insight on the Pr^{3+}/CAC molecular interaction within the matrix gate through energy minimization steps*

The analyses performed on BAC matrix gate acidic residues has been also carried out on CAC. Praseodymium trivalent cation was manually moved within 3 Å of negatively charged residues D32, E132 and D231, which are the homologous of respectively D23, E114 and D211 of BAC. Four steps of energy minimization were thus performed on the homology model of the carnitine carrier, as follows: 1) crystal structure of the empty carnitine carrier. After 250 step of energy minimization, the total energy of the system was equal to −10,181.00 kcal/mol. In this conformation, the salt bridge between D32-K135, D231-K35 and E132-K234 occurred as shown, Fig. 1E; 2) complex of carrier and Pr^{3+}, the latter placed within 3 Å of D32 residue, Fig. 6A–D; 3) complex of carrier and Pr^{3+}, the latter placed within 3 Å of E132 residue Fig. 6B–E; and 4) complex of carrier and Pr^{3+}, the latter placed within 3 Å of D231 residue Fig. 6C–F. Energy minimizations were performed with Prime package available on Schrodinger suite as described in Materials and methods section. The second energy minimization was run after positioning the Pr^{3+} cation within 3 Å from D32 residue. Interestingly, the K135 side-chain was displaced for the likely occurrence of electrostatic repulsive

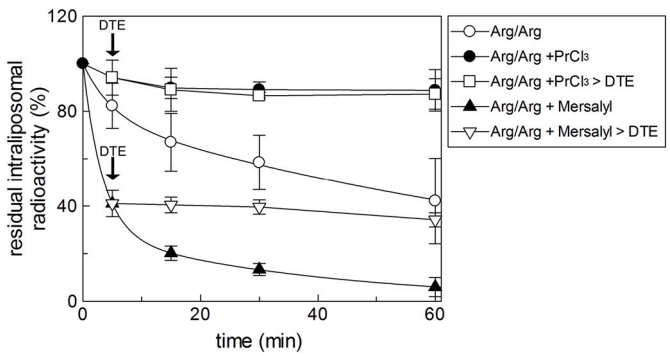

Fig. 4. Effect of $PrCl_3$ on the arginine efflux from proteoliposomes. Efflux of 15 mM [^{3}H]arginine efflux from pre-labeled proteoliposomes was measured at the indicated times in the presence of external 5 mM arginine (○), 5 mM arginine with 5 mM $PrCl_3$ (●), 5 mM arginine with 0,5 mM mersalyl (▲). 5 min after the start, as indicated by the arrows, 5 mM DTE was added both to the proteoliposomes pretreated with $PrCl_3$ (□) and with mersalyl (△). The values are means ± SD from three experiments.

interactions with Pr^{3+} cation, Fig. 6A. As a result, side chain of D32, and carbonyl backbone of H29 and Q139 can be involved to coordinate the Pr^{3+} cation, Fig. 6D. Total energy of the system after 250 energy minimization steps was equal to −10,278.58 kcal/mol. The third energy minimization was carried out by positioning the Pr^{3+} cation within 3 Å from E132 residue, Fig. 6B. Interestingly, the D179 residue, which is normally placed at about 9 Å with respect to E132, was instead rotated to play attractive interactions with Pr^{3+}, Fig. 6E. Total energy of for this minimization was equal to −10,423.12 kcal/mol, which is the best energetic sampled value. The last energy minimization was carried out by moving the Pr^{3+} cation within 3 Å of D231 residue. Again, the lysine residue K35, which normally formed salt bridge with D231, moved away for the presence of Pr^{3+} cation, Fig. 6C. Side chain of carboxyl group of D231 and carbonyl backbone groups of Q39 and A227 are involved in the flagged coordination bond with the Pr^{3+} cation, Fig. 6F. Total energy system after energy minimization was equal to −10,323.79 kcal/mol.

3.5. *Insight on putative interactions between carriers and Pr^{3+} based on unbiased simulations*

For reasons of completeness, further simulations of BAC and CAC in complex with Pr^{3+} ion were performed. More specifically, we carried out ten independent simulations for each protein-ion complex. The ion was initially placed in the center of the matrix gate, within about 6 Å of residues D23, D211 and E114 of BAC and D32, D231 and E132 of CAC. After that, the ion was moved along the z-axis in ten different positions and an energy minimization was run. More specifically, starting from the initial coordinates of the Pr^{3+}, the cation was moved on the top and on the bottom from the matrix gate with a step of about 4 Å along the z-axis. Such simulations allowed us to avoid bias towards specific residues and to better sample the occurrence of possible interactions between Pr^{3+} and carriers (Fig. S1 of Supporting Information). Eventually, we searched for other potential regions with high density of negative charged residues where Pr^{3+} cation could be placed as suggested by Deepview Alphafold [27]. In this respect, we sampled by simulations two further sites characterized by several negatively charged residues. For both the carriers, these sites are in proximity of the mitochondrial matrix (Figs. S2 and S3 of Supporting Information).

4. Discussion

The availability of specific inhibitors for enzymes as well as for transport proteins, represents a fundamental tool for a biochemist. Thanks to effective and fast inhibitors, it is possible to perform accurate biochemical protein characterization. Inhibitors which block the

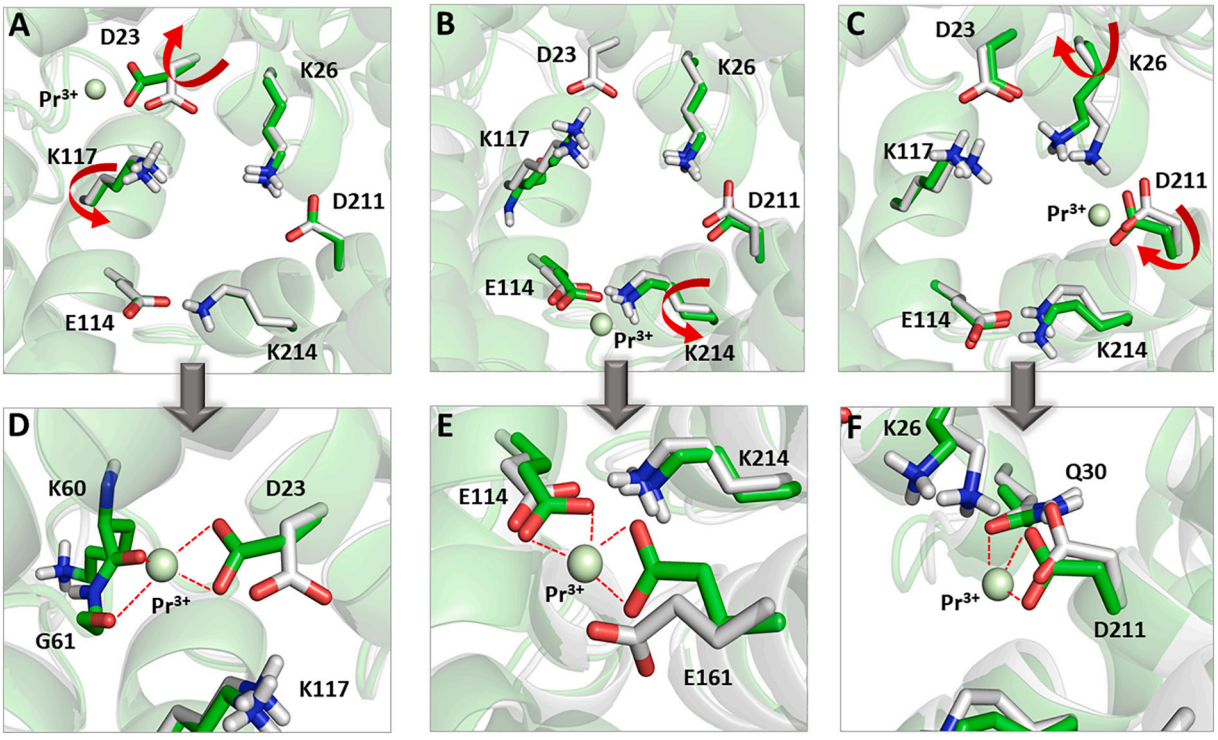

Fig. 5. Interaction of Pr^{3+} with BAC acidic matrix salt bridge network amino acids.
In panels (A), (B) and (C) are shown the overlaps between the empty BAC carrier (depicted in white) and BAC-D23-Pr^{3+}, BAC-D211-Pr^{3+} and BAC-E114-Pr^{3+} complexes (depicted in green), with red arrows indicating the displacement of residues driven by the presence of Pr^{3+} ion. Panels (D), (E) and (F) report the zoom at the residues involved in the coordination where are also evident the other residues involved in Pr^{3+} interaction. Red dashed lines show coordination bonds of protein residues with praseodymium ion. (For interpretation of the references to color in this figure legend, the reader is referred to the web version of this article.)

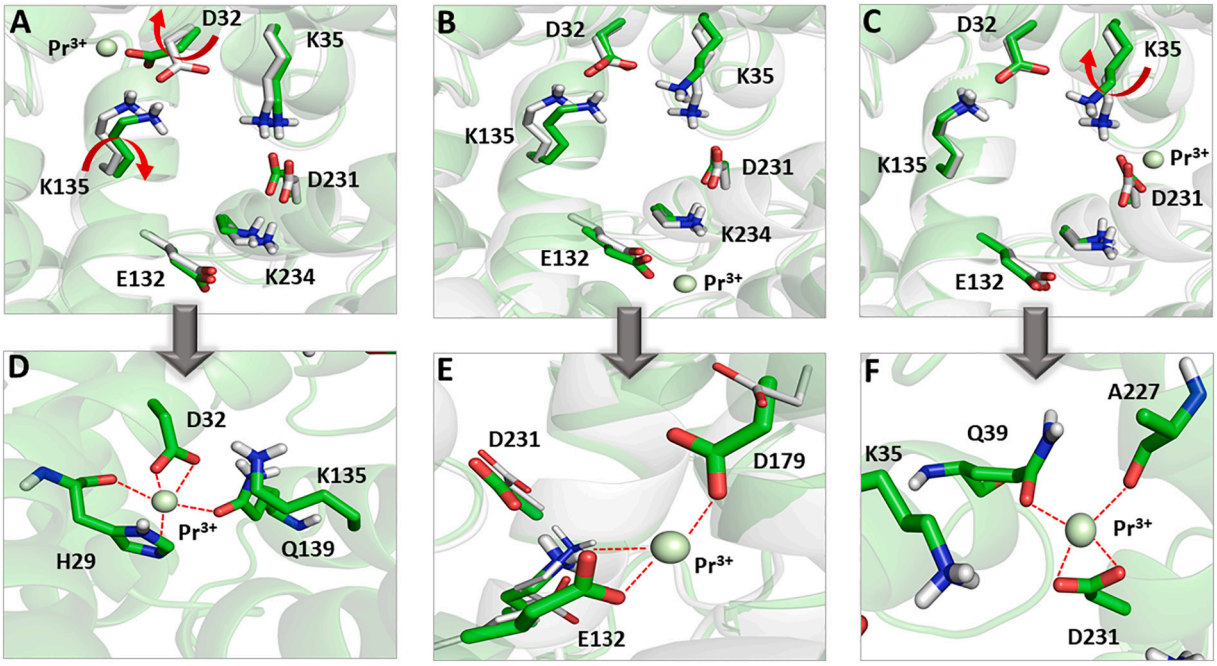

Fig. 6. Interaction of Pr^{3+} on CAC acidic matrix salt bridge network amino acids.
Panels (A), (B) and (C) are shown the overlaps between the empty CAC carrier (depicted in white) and CAC-D32-Pr^{3+}, CAC-E132-Pr^{3+} and CAC-D231-Pr^{3+} complexes (depicted in green) and red arrows indicating the displacement of residues driven by the presence of Pr^{3+} ion. Panels (D), (E) and (F) report zoom at the residues involved in the coordination where are also evident the other residues involved in Pr^{3+} interaction. Red dashed lines show coordination bonds with praseodymium ion. The CAC-praseodymium complex has been represented by using the molecular visualization program PyMOL. (For interpretation of the references to color in this figure legend, the reader is referred to the web version of this article.)

mitochondrial transporters (MCF) in a specific conformation without modifying their structure are also essential for crystallization studies. Some widely used inhibitors of MCF are thiol reagents (mersalyl, p-chloromercuribenzenesulfonate, mercuric chloride, and N-ethylmaleimide), the lysine reagent pyridoxal 5-phosphate (PLP) as well as bathophenanthroline, α-cyanocinnamate and bromocresol purple, whose mechanism of action are still partially unknown. Moreover, mercurial reagents at concentration higher than 10–500 μM can induce the switch of the transporter to a "pore-like" structure in several Slc25 members. Despite numerous papers which address this topic, no clear explanation of the protein alteration at molecular level is available, indicating that mercurials must be used with awareness [33,39]. Other than generic protein blockers, specific inhibitors for a single transporter have been found; for example, ANT is effectively blocked in two different conformations, c-state and m-state respectively by (C)ATR and BKA. Even though essential for the crystallization process (CATR/ANT), these inhibitors can slightly modify the protein conformation due to their steric hindrance. In this work we demonstrated that $PrCl_3$ does inhibit the transport activity catalyzed by a subset of related mitochondrial carriers. We set to test its efficacy on the reconstituted human recombinant transporters ORC1, BAC and CAC also taking advantage of the right-side-out orientation of the transporters in the proteoliposomal bilayer [34,35]. We observed that Pr^{3+} inhibits the three human mitochondrial carriers ORC1, BAC and CAC with IC_{50} values in the micromolar range, respectively of 522 ± 62 μM, 52.5 ± 8.8 μM and 155 ± 17 μM, and completely blocks their transport activity at 2–5 mM. Investigation was deepened on BAC and CAC, which were the more sensitive carriers. From kinetic experiments, we obtained the K_i values for Pr^{3+}: 28.5 ± 11.7 μM for BAC and 257.7 ± 71.6 μM for CAC and demonstrated that Pr^{3+} is a competitive inhibitor for both the carriers. The difference of IC_{50} and Ki among the two mitochondrial carriers reflects Pr^{3+} tendency to create more, and different coordination bonds in BAC respect to CAC in crucial portions of the translocator such as the active binding site and the salt bridge in the c-state conformation (see Figs. 5, 6, S1, S2, S3).

Starting from this information, and looking at the substrate's characteristic, we point our studies on the amino acid(s) involved in Pr^{3+} interaction. Both the translocators have a negative charge interacting with the substrate, CAC-D179 binds carnitine's trimethylammonium [20] and likely BAC-E161 binds both its transported substrate, arginine's guanidine group, or the primary amino group of lysine [21,40] (Fig. 1C, F, green residues). Moreover there is another common MCF feature that could be involved with the carrier's interaction with Pr^{3+}, the negative residues of the matrix salt bridge network constituted by the third and sixth conserved charged residues of the Px[***DE***]xx[**KR**] signature motifs, present in the odd numbered α-helices, which interact during the catalytic process, see introduction. This charge network is located just below the substrate binding site, as clearly evident in the lateral view representation in Fig. 1C, F [2]. We propose that the acidic residues, participating to the salt bridge network (Fig. 1B, E), can also be the praseodymium target. These residues protrude into the water filled cavity delimited by six α-helical bundle opened towards the cytosol and are highlighted in Fig. 1A, D where BAC and CAC are depicted in the c-state and the water-filled cavity is more evident. We here also employed a computational approach to predict the putative interaction between praseodymium ion with the negatively charged residues in the attempt to elucidate, at a molecular level, praseodymium inhibition. Interestingly, minimization cycles for each Pr^{3+}/BAC and Pr^{3+}/CAC systems allowed to spot the most probable site of praseodymium ion for better interacting with different side chains conformation with lowest energy. Interaction of Pr^{3+} with CAC-E132 or with BAC-E114 (Figs. 5, 6) gave the lowest energy level, thus suggesting that these are the most prone to Pr^{3+} coordination. This is also supported by their higher accessibility from the cytosol, in the carrier's water filled cavity, Fig. 1A–D. It is interesting to note that from the computational analyses of CAC both H29 and D179, which are involved in the substrate binding during the transport catalysis [20,41], are coordinated by praseodymium accordingly with the competitive nature of the inhibition, Fig. 6D and E. This let us to confirm that E161, which is homologous with D179, is part of

the BAC active site Fig. 5E. Overall, the electrostatic charge of Pr^{3+} cation can attract several residues along with the catalytic ones. In particular, the backbone carbonyl groups, or the imidazole ring of histidine residues can participate to the coordination and thus to the stabilization of the ion within carriers, Fig. 6D. In addition, unbiased simulations deployed in water-filled cavities of BAC and CAC (Fig. S1 of SI) demonstrated the pivotal role of matrix-gate and binding site acidic residues for effective binding of the Pr^{3+} cation. Noteworthy, all the coordination bonds are automatically flagged by GLIDE software as mentioned above in agreement with a number of X-ray solved structures containing Pr^{3+} cation available from the Cambridge Crystallographic Data Center [42]. The unbiased simulations (Fig. S1 of SI), can also explain the higher BAC's sensitivity to the lantanide since the double coordination between the corresponding E132 and D179 residues in CAC was not detected in these unbiased simulations, probably due to the aspartate shorter side chain. Even though the previsions from computational analyses pointed to E132 as the most favored CAC's residue to Pr^{3+} coordination, unfortunately its substitution, as well as of any of the acidic residues, either of the active site or of the matrix gate, almost completely inactivates CAC. This points to the importance of "each" of the negative charges as reported by Giangregorio et al. [20] and does not allow to confirm results obtained from computational analyses through experiments using mutant proteins. To exclude any praseodymium "side effect" such as a specific proteoliposomes permeabilization and triggering of the "pore like" switch of the carrier, it has been performed a backward exchange experiment, efflux of radiolabeled substrate from actively preloaded proteoliposomes, on BAC. Pr^{3+} completely inhibits the efflux of labeled substrate (Fig. 3) and does not cause any unspecific efflux, even used at high concentration (5 mM), neither perturbing the phospholipid bilayer nor inducing the "pore-like" switch phenomenon that occurs in several MCF members in the presence of several metals and mercurials and whose molecular cause is still elusive. Pr^{3+} inhibition is not reversed by DTE indicating that it does not coordinate any cysteine according to its chemical properties. In fact, being Pr^{3+} a hard acceptor in HSAB sense, it is expected to form a hard-hard acid-base pair. In the scale from hard to soft base we found O > N > S atoms, that explains the strong preference of Pr^{3+} for oxygen donor ligands as shown by modeling investigations (Fig. 5 and Fig. 6) as well as why it is not engaged in coordination with cysteine. Based on the HSAB concept, the sulfhydryl group of a cysteine residue is a soft base and thus the affinity of Pr^{3+} for the soft base is low. In the backward experiments we also, for the first time, evidenced that mersalyl 0.5 mM, triggers the "pore-like" switch of BAC, thus also Slc25A29 it can be included in the MCF subgroup that is structurally altered by mercury derivatives [33,37,39,43]. We also tested aluminum trivalent ion ($AlCl_3$) but even though we measured an IC_{50} value of about 1 mM, it was then demonstrated that its effect was the specific perturbation of the proteoliposomal scaffold. Other trivalent cations such as Sb^{3+} and As^{3+} have not been considered in this study since they have been already analyzed in previous researches which demonstrated that they reversibly react with CAC's cysteine [44]. Divalent cations effects on CAC and ORC1 have also been already studied in previous works, where it was analyzed their effectiveness and reversibility as their capability to induce the "pore-like" switch of the carriers [22,33,39]. As well known, the limiting step from protein to structure is its crystal production. Achieving membrane protein crystals is far more difficult than soluble proteins and an inhibitor is mandatory for its crystallization [1]. The finding of state-specific binders is an elegant way to obtain a desired conformational state [45]. Pr^{3+}, efficiently inhibits the proteins tested probably in the c-state, when the negative charges of the gate are available from the cytosol. Moreover, being Pr^{3+} characterized by small dimension (radius: 0.99 Å) and hindrance it should induce only slight protein structural modification. This feature can point to Pr^{3+} as an elective inhibitor for crystallization and structural studies, at least for BAC, ORC1 and CAC, as well as other proteins that can be blocked by the metal. The crystallographic approach can, for example, definitively clarify every molecular aspect of CAC, which is one of the most studied at the molecular level, among the MCF and whose active site has been accurately mapped thanks to mutagenic and bioinformatics approaches [46]. This should moreover clarify the molecular determinants responsible of switch between uniport and antiport since it is the only in the MCF catalyzing both these activities.

5. Conclusions

In this paper we have reported that Pr^{3+} behaves as a new competitive inhibitor both for the human mitochondrial basic amino acid (BAC, ORC1) and carnitine/acylcarnitine (CAC) transporters. It could be hypothesized that praseodymium represents a useful tool for functional studies of other Pr^{3+} sensitive mitochondrial carriers, as stop inhibitor. This lanthanide metal is classified as "hard Lewis acids" [14], and forms a strong interaction with negatively charged amino acids. Here, it has been demonstrated it's binding to the matrix salt bridge network negative residues, close to the substrate binding site in the c-state, with the subsequent block of the carriers in this conformation. Since this charged network (matrix-gate) is common to all mitochondrial carriers, Besides, Pr^{3+} is potentially useful for structural studies based on crystallographic approach, also of other members of MCF and its small size that should not alter the translocator structure, can be considered its additional value.

Funding

This work was supported by PRIN (Progetti di Ricerca di Interesse Nazionale) project n. 2017PAB8EM MIUR (Italian Ministry of Instruction, University and Research).

Declaration of competing interest

The authors declare that they have no known competing financial interests or personal relationships that could have appeared to influence the work reported in this paper.

Appendix A. Supplementary data

Supplementary data to this article can be found online at https://doi.org/10.1016/j.bbabio.2022.148557.

References

[1] J. Li, R. Abel, K. Zhu, Y. Cao, et al., The VSGB 2.0 model: a next generation energy model for high resolution protein structure modeling, Proteins 79 (10) (Oct 2011) 2794–2812.
[2] C. Indiveri, A. Tonazzi, A. de Palma, F. Palmieri, Kinetic mechanism of antiports catalyzed by reconstituted ornithine/citrulline carrier from rat liver mitochondria, Biochim. Biophys. Acta Bioenerg. 1503 (3) (2001) 303–313. JAN 19 2001.
[3] I. Jona, A. Martonosi, The effects of membrane potential and lanthanides on the conformation of the Ca2+-transport ATPase in sarcoplasmic reticulum, Biochem. J. 234 (2) (1986) 363–371.
[4] C. Indiveri, A. Tonazzi, T. Dierks, R. Krämer, et al., The mitochondrial carnitine carrier: characterization of SH-groups relevant for its transport function, Biochim. Biophys. Acta 1140 (1) (Nov 1992) 53–58.
[5] V. Porcelli, G. Fiermonte, A. Longo, F. Palmieri, The human gene SLC25A29, of solute carrier family 25, encodes a mitochondrial transporter of basic amino acids, J. Biol. Chem. 289 (19) (May 2014) 13374–13384.
[6] H.M. Berman, J. Westbrook, Z. Feng, G. Gilliland, et al., The protein data Bank, Nucleic Acids Res. 28 (1) (Jan 2000) 235–242.
[7] N. Giangregorio, A. Tonazzi, L. Console, C. Indiveri, et al., Site-directed mutagenesis of charged amino acids of the human mitochondrial carnitine/acylcarnitine carrier: Insight into the molecular mechanism of transport, Biochim. Biophys. Acta Bioenerg. 1797 (6-7) (2010) 839–845. JUN-JUL 2010.
[8] T. Dierks, A. Salentin, R. Krämer, Pore-like and carrier-like properties of the mitochondrial aspartate/glutamate carrier after modification by SH-reagents: evidence for a performed channel as a structural requirement of carrier-mediated transport, Biochim. Biophys. Acta 1028 (3) (Oct 1990) 281–288.
[9] C. Indiveri, V. Iacobazzi, N. Giangregorio, F. Palmieri, Bacterial overexpression, purification, and reconstitution of the carnitine/acylcarnitine carrier from rat liver mitochondria, Biochem. Biophys. Res. Commun. 249 (3) (Aug 1998) 589–594.

[10] A. Tonazzi, N. Giangregorio, L. Console, M. Scalise, et al., Mitochondrial carnitine/acylcarnitine transporter, a novel target of mercury toxicity, Chem. Res. Toxicol. 28 (5) (May 2015) 1015–1022.
[11] P. Benkert, M. Künzli, T. Schwede, QMEAN server for protein model quality estimation, Nucleic Acids Res. 37 (Web Server issue) (Jul 2009) W510–W514.
[12] C. Indiveri, A. Tonazzi, F. Palmieri, The reconstituted carnitine carrier from rat liver mitochondria: evidence for a transport mechanism different from that of the other mitochondrial translocators, Biochim. Biophys. Acta 1189 (1) (Jan 1994) 65–73.
[13] C. Indiveri, A. Tonazzi, N. Giangregorio, F. Palmieri, Probing the active site of the reconstituted carnitine carrier from rat liver mitochondria with sulfhydryl reagents. A cysteine residue is localized in or near the substrate binding site, Eur. J. Biochem. 228 (2) (Mar 1995) 271–278.
[14] A. Pasquadibisceglie, F. Polticelli, Structural determinants of ligands recognition by the human mitochondrial basic amino acids transporter SLC25A29. Insights from molecular dynamics simulations of the c-state, Comput. Struct. Biotechnol. J. 19 (2021) 5600–5612.
[15] M.P. Jacobson, D.L. Pincus, C.S. Rapp, T.J. Day, et al., A hierarchical approach to all-atom protein loop prediction, Proteins 55 (2) (May 2004) 351–367.
[16] Schrödinger Release Prime, Schrödinger, New York. https://www.schrodinger.com/platform, 2020, 4.
[17] Kenjiro Yazawa, Michihiro Sugahara, Katsuhide Yutani, Michiyo Takehira, et al., Derivatization of proteinase K with heavy atoms enhances its thermal stability, ACS Catal. 6 (5) (2016) 3036–3046.
[18] C.collab <collab>S.V., Lanthanide And Actinide Chemistry, in: A Wiley Series of Advanced Textbooks, John Wiley & Sons Ltd, The Atrium, Southern Gate, Chichester, West Sussex PO19 8SQ, England, 2006, 0-470-01005-3.
[19] R.G. Pearson, Hard and soft acids and bases, HSAB, Part I, J. Chem. Educ. 45 (9) (1968) 581–587.
[20] A.J. Robinson, C. Overy, E.R. Kunji, The mechanism of transport by mitochondrial carriers based on analysis of symmetry, Proc. Natl. Acad. Sci. U. S. A. 105 (46) (Nov 2008) 17766–17771.
[21] E. Harder, W. Damm, J. Maple, C. Wu, et al., OPLS3: a force field providing broad coverage of drug-like small molecules and proteins, J. Chem. Theory Comput. 12 (1) (Jan 2016) 281–296.
[22] E.R.S. Kunji, M.S. King, J.J. Ruprecht, C. Thangaratnarajah, The SLC25 carrier family: important transport proteins in mitochondrial physiology and pathology (09 01), Physiology (Bethesda) 35 (5) (2020) 302–327.
[23] F. Palmieri, C. Indiveri, F. Bisaccia, V. Iacobazzi, Mitochondrial metabolite carrier proteins: purification, reconstitution, and transport studies, Methods Enzymol. 260 (1995) 349–369.
[24] A. Tonazzi, C. Indiveri, Chemical modification of the mitochondrial ornithine/citrulline carrier by SH reagents: effects on the transport activity and transition from carrier to pore-like function, Biochim. Biophys. Acta Biomembr. 1611 (1-2) (2003) 123–130. APR 1 2003.
[25] J.J. Ruprecht, E.R.S. Kunji, The SLC25 mitochondrial carrier family: structure and mechanism, Trends Biochem. Sci. 45 (3) (2020) 244–258, 03.
[26] E. Pebay-Peyroula, C. Dahout-Gonzalez, R. Kahn, V. Trézéguet, et al., Structure of mitochondrial ADP/ATP carrier in complex with carboxyatractyloside, Nature 426 (6962) (Nov 2003) 39–44.
[27] R.G. Pearson, Hard and soft acids and bases, J. Am. Chem. Soc. 85 (Physical and Inorganic Chemistry) (1963) 3533–3539.
[28] R.G. Pearson, Hard and soft acids and bases, HSAB, J. Chem. Educ. Part II 45 (10) (1968) 643–648.
[29] N. García, E. Martínez-Abundis, N. Pavón, F. Correa, et al., Copper induces permeability transition through its interaction with the adenine nucleotide translocase, Cell Biol. Int. 31 (9) (Sep 2007) 893–899.
[30] N. Giangregorio, A. Tonazzi, L. Console, M. Galluccio, et al., Structure/function relationships of the human mitochondrial ornithine/citrulline carrier by Cys site-directed mutagenesis. Relevance to mercury toxicity, Int. J. Biol. Macromol. 120 (Pt A) (Dec 2018) 93–99.
[31] M. Scalise, L. Pochini, N. Giangregorio, A. Tonazzi, et al., Proteoliposomes as tool for assaying membrane transporter functions and interactions with xenobiotics, Pharmaceutics 5 (3) (2013) 472–497.
[32] C. Indiveri, A. Tonazzi, F. Palmieri, Identification and purification of the ornithine/citrulline carrier from rat liver mitochondria, Eur. J. Biochem. 207 (2) (Jul 1992) 449–454.
[33] F. Palmieri, P. Scarcia, M. Monné, Diseases caused by mutations in mitochondrial carrier genes, Biomolecules 10 (4) (2020), 04 23.
[34] F. Palmieri, C.L. Pierri, A. de Grassi, A. Nunes-Nesi, et al., Evolution, structure and function of mitochondrial carriers: a review with new insights, Plant J. 66 (1) (Apr 2011) 161–181.
[35] T.D. Singh, C. Sumitra, G. Bag, et al., Molecular and biomolecular spectroscopy, Spectrochim. Acta A 63 (1) (2006) 154–159.
[36] S. Gharouel, L. Labrador-Páez, A. Urbieta, P. Fernández, et al., Luminescence and cathodoluminescence properties of MIPr(PO3)4 (MI =Na, Li, K) and PrP5O14, Phys. B Condens. Matter 554 (2019) 121–125, research article.
[37] M. Klingenberg, M. Appel, W. Babel, H. Aquila, The binding of bongkrekate to mitochondria, Eur. J. Biochem. 131 (3) (1983) 647–654.
[38] J.J. Ruprecht, M.S. King, T. Zögg, A.A. Aleksandrova, et al., The molecular mechanism of transport by the mitochondrial ADP/ATP carrier, Cell 176 (3) (2019) 435–447.e415, 01.
[39] G. Studer, M. Biasini, T. Schwede, Assessing the local structural quality of transmembrane protein models using statistical potentials (QMEANBrane), Bioinformatics 30 (17) (2014) i505–i511.
[40] J. Jumper, R. Evans, A. Pritzel, T. Green, et al., Highly accurate protein structure prediction with AlphaFold, Nature 596 (7873) (Aug 2021) 583–589.
[41] M.A. Seeger, Membrane transporter research in times of countless structures, Biochim. Biophys. Acta Biomembr. 1860 (4) (2018) 804–808. Apr.
[42] R. Krämer, C. Heberger, Functional reconstitution of carrier proteins by removal of detergent with a hydrophobic ion exchange column, Biochim. Biophys. Acta 863 (2) (Dec 1986) 289–296.
[43] A. Tonazzi, N. Giangregorio, L. Console, F. Palmieri, et al., The mitochondrial carnitine acyl-carnitine carrier (SLC25A20): molecular mechanisms of transport, role in redox sensing and interaction with drugs, Biomolecules 11 (4) (2021) 03 31.
[44] A. Tonazzi, N. Giangregorio, C. Indiveri, F. Palmieri, Identification by site-directed mutagenesis and chemical modification of three vicinal cysteine residues in rat mitochondrial carnitine/acylcarnitine transporter, J. Biol. Chem. 280 (20) (2005) 19607–19612. MAY 20 2005.
[45] A. Tonazzi, C. Indiveri, Effects of heavy metal cations on the mitochondrial ornithine/citrulline transporter reconstituted in liposomes, Biometals 24 (6) (2011) 1205–1215. DEC 2011.
[46] C.R. Groom, I.J. Bruno, M.P. Lightfoot, S.C. Ward, The Cambridge structural database, Acta Crystallogr. B Struct. Sci. Cryst. Eng. Mater. 72 (Pt 2) (Apr 2016) 171–179.